2019-05-09

Numerical Investigation into the Effect of Sound Speed in Attached Cavitation on Hydrofoil Modes of Vibration

Wang, W

10.3390/en12091758
Energies
MDPI

energies

MDPI

Article

Numerical Investigation into the Effect of Sound Speed in Attached Cavitation on Hydrofoil Modes of Vibration

Wei Wang [1], Lingjiu Zhou [1,2,*], Zhengwei Wang [3], Xavier Escaler [4] and Oscar De La Torre [5]

1 College of Water Resources and Civil Engineering, China Agricultural University, Beijing 100091, China; wweizn@163.com
2 Beijing Engineering Research Center of Safety and Energy Saving Technology for Water Supply Network System, Beijing 100000, China
3 Department of Thermal Engineering, Tsinghua University, Beijing 100091, China; wzw@mail.tsinghua.edu.cn
4 Department of Fluid Mechanics, Universitat Politècnica de Catalunya-Barcelona Tech, 08028 Barcelona, Spain; xavier.escaler@upc.edu
5 School of Marine Science and Engineering, Plymouth University, Plymouth PL4 8AA, UK; oscar.delatorre@plymouth.ac.uk
* Correspondence: zlj@cau.edu.cn

Received: 16 April 2019; Accepted: 6 May 2019; Published: 9 May 2019

Abstract: It has been found recently that the dynamic behavior of a cavitating hydrofoil is different from that in pure water in that, not only are the natural frequencies different, but the mode shapes may also change. In order to elucidate the mechanism behind this phenomenon, finite element simulations were carried out based on acoustic–structure coupling equations. It was found that the structure and acoustic modes exhibit mode transitions with the variation of the sound speed in the cavity. Further, the mode transition was caused by coupling of the structure with the acoustic modes, which was induced by the vapor mode. The amplitude of the vibration near the mode transition point was high and the mode shape was easily excited. Moreover, with the change of the sound speed in the cavity, the different distributions of the acoustic pressure mode resulted in different structure mode shapes, even on the same transition line. Considering this, a sheet cavitation was simulated by a small change of the void fraction to 0.999 and the sound speed from 343 to 275 m/s to obtain good agreement with the experimental data. Both results showed that the second bending mode under cavitation conditions became a bending–torsion coupled mode.

Keywords: hydrofoil; natural frequencies; mode shapes; sound speed; cavitation

1. Introduction

In response to worldwide concerns over fossil fuel consumption and global warming, renewable energy technologies have become increasingly favored as alternative natural energy resources. Among these, tidal power is relatively predictable as it is nearly periodic, occurring twice a day in most areas and once a day in some places, and has calculable fluctuations over the solar and lunar cycle. Tidal barrage and tidal stream stations are two of the main types of commercial scale stations. In both cases, cavitation on the runner might cause severe energy drop and even damage to the runner; as such, considerable efforts have been made to understand this phenomenon. However, recent research shows that cavitation may change the dynamic response of submerged structures, since the properties of the surrounding liquid can easily change when cavitation appears (i.e., the speed of sound and density). This has been rarely referred to in past research on tidal turbines. Recently, Liu et al. [1] found that the value of the speed of sound inside the cavity had a significant influence on the structure modes of

vibration, while the effect of changing the density was negligible. So, it is very important to correctly assess the dynamic behavior of hydraulic machinery under cavitation conditions during the design stage to avoid resonances.

The study of the added mass effect on the dynamic behavior of the structure mainly focuses on two aspects of natural frequencies and mode shapes [2–4]. Many researchers, such as Lindholm et al. [5], Kwak [6], Chang and Liu [7], and Rodriguez et al. [8], have conducted experimental and numerical investigations in plates and complex structures in water conditions. They found that the natural frequencies of submerged structures reduce significantly due to the added mass effect. Meanwhile, Ergin and Ugurlu [8] experimentally found that the wet frequencies decrease as the submergence depth increases. Dompierre et al. [9] and Rodriguez et al. [10] studied the influence of nearby rigid surfaces on wet natural frequencies. Valentín et al. [11] demonstrated that fluid density is one of the most important parameters for determining the decrease of natural frequencies.

In summary, all these studies have shown that the natural frequencies of a structure submerged in a homogeneous and high density fluid, e.g., water, are drastically reduced. However, the surrounding conditions can easily change for hydraulic machinery when cavitation appears. Cavitation on propellers can not only result in thrust drop and vibration damage to stability, it can also produce large volumes of vapor that are usually close to the solid boundaries; thus, the structure is not fully wetted and the surrounding fluid is not homogeneous. In spite of that, visual observations during experiments in cavitation tunnels showed that the macroscopic cavity sheet is in fact composed of a mixture of liquid and vapor phases with averaged properties that vary from those expected of pure vapor. However, few studies have been done regarding the modal response of a submerged body surrounded by cavitation. For instance, Fine et al. [12] found that the added mass of a circular disk under supercavitation is lower than when under fully wetted conditions.

Recent experimental research by De La Torre et al. [13–15] was devoted to investigating the modal response of a 2-D NACA0009 truncated hydrofoil under partial cavitation conditions. The results confirmed that the added mass effects decreased relative to the fully wetted condition as the cavity length increased. Moreover, it was found that the mode shape deformation and the location of the nodal lines for the three first modes of vibration were dependent on the fluid conditions and, in particular, significant alterations were found under cavitation conditions. It was found that the mode shape of the second bending mode under cavitation conditions was actually a bending–torsion coupled mode. However, it is unclear why the bending–torsion coupled mode appears.

A preliminary evaluation of its sensitivity to the values of the cavity average properties was carried out by Liu et al. [16] using a FEM (Finite Element Method) model. Briefly, it was found that the speed of sound in the cavity could have a significant effect both on the frequencies and the mode shapes, while the effect of changing the density was negligible. More specifically, all the natural frequencies suffered a linear decrease in a particular range of sonic velocities, forming a common diagonal line for all the modes which we refer to as the "mode transition line". However, the reason for the so-called "mode transition" has not been clarified in previous papers. Consequently, the work in this paper is devoted to clarifying this surprising numerical behavior and understanding the mode transition phenomenon. The numerical mode is shown in Section 2. In Section 3, the influence of the speed of sound (c_c) on the first three structure modes is analyzed in reference to Liu et al.'s [1] work. To do so, attention has been given to the possible influence of the acoustic frequencies of the fluid domain. Such an effect has been recently demonstrated by Bossio et al. [17] on the natural frequencies of a submerged hydrofoil. Then, the influence of c_c on the acoustic modes is shown in the Section 4, which provides a good explanation for the mode transition phenomenon discussed in the Section 5. Finally, the reason for the appearance of the bending–torsion coupled mode is further discussed in real cavitation conditions in Section 6, and the conclusions are summarized in Section 7.

2. Numerical Mode

2.1. Acoustic Fundamentals

A commercial code of ANSYS Workbench® version 12.0 (12.0, ANSYS Inc., Pennsylvania, USA) is used in present work. The structure dynamic behavior in matrix notation can be described as:

$$[M_s]\{\ddot{u}\} + [C_s]\{\dot{u}\} + [K_s]\{u\} = \{F_s\} \tag{1}$$

where $[M_s]$ is the structural mass matrix, $[C_s]$ is the structural damping matrix, $[K_s]$ is the structural stiffness matrix, $\{F_s\}$ is the load vector, and $\{u\}$ is the nodal displacement vector.

When the structure is submerged in the fluid, $\{F_s\}$ is caused by the pressure distribution of the fluid. The pressure distribution is determined using the acoustic wave equation, which considers the fluid as inviscid, irrotational, and with no mean flow:

$$\nabla \cdot \left(\frac{1}{\rho_0}\nabla P\right) - \frac{1}{\rho_0 c^2}\frac{\partial^2 P}{\partial t^2} + \nabla \cdot \left[\frac{4\mu}{3\rho_0}\nabla\left(\frac{1}{\rho_0 c^2}\frac{\partial P}{\partial t}\right)\right] = -\frac{\partial}{\partial t}\left(\frac{Q}{\rho_0}\right) + \nabla \cdot \left[\frac{4\mu}{3\rho_0}\nabla\left(\frac{Q}{\rho_0}\right)\right] \tag{2}$$

where $c = \sqrt{K/\rho_0}$ is speed of sound, ρ_0 is mean density, K is bulk modulus, μ is dynamic viscosity, P is acoustic pressure, Q is mass source in the continuity equation, t is time.

The finite element formulation of the wave equation is obtained by testing wave using the Galerkin procedure:

$$\begin{aligned} &\iiint_{\Omega_f} \tfrac{1}{\rho_0 c^2} w \tfrac{\partial^2 P}{\partial t^2} dv + \iiint_{\Omega_f} \nabla w \cdot \left(\tfrac{4\mu}{3\rho_0^2 c^2}\nabla \tfrac{\partial P}{\partial t}\right) dv + \iiint_{\Omega_f} \nabla w \cdot \left(\tfrac{1}{\rho_0}\nabla P\right) dv \\ &+ \oiint_{\Gamma_f} w \hat{n} \cdot \tfrac{\partial^2 \vec{u}_f}{\partial t^2} ds = \iiint_{\Omega_f} w \tfrac{1}{\rho_0}\tfrac{\partial Q}{\partial t} dv + \iiint_{\Omega_f} \nabla w \cdot \left(\tfrac{4\mu}{3\rho_0^2}\nabla Q\right) dv \end{aligned} \tag{3}$$

where: dv is volume differential of acoustic domain Ω_f, ds is surface differential of acoustic domain boundary Γ_f, $\hat{n}$ is outward normal unit vector to the boundary Γ_f, $\vec{u}_f$ is the displacement of the fluid particle.

The fluid pressure p and the structural displacement components $\vec{u}_F$ are the dependent variables from Equation (3), P and $\vec{u}_F$ can be obtained respectively by the finite element approximating shape functions.

$$P = \{N\}^T\{p\} \tag{4}$$

$$u = \{N'\}^T\{u_e\} \tag{5}$$

where: $\{N\}$ is element shape function for pressure, $\{N'\}$ is element shape function for displacements, $\{p\}$ = nodal pressure vector, $\{u_e\} = \{u_{xe}\}$, $\{u_{ye}\}$, $\{u_{ze}\}$ is nodal displacement component vectors.

The finite element formulation of the wave equation can be also expressed as:

$$\begin{aligned} &\iiint_{\Omega_f} \tfrac{1}{\rho_0 c^2}\{N_p\}\{N_p\}^T dv\{\ddot{p}\} + \iiint_{\Omega_f} \tfrac{4\mu}{3\rho_0^2 c^2}[\nabla N_p]^T[\nabla N_p] dv\{\dot{p}\} + \iiint_{\Omega_f} \tfrac{1}{\rho_0}[\nabla N_p]^T[\nabla N_p] dv\{p\} \\ &+ \oiint_{\Gamma_f} \{N_p\}\{n\}^T\{N'_p\}^T ds\{\ddot{u}_{e,f}\} = \iiint_{\Omega_f} \tfrac{1}{\rho_0}\{N_p\}\{N_p\}^T dv\{\dot{q}\} + \iiint_{\Omega_f} \tfrac{4\mu}{3\rho_0^2 c^2}[\nabla N_p]^T[\nabla N_p] dv\{q\} \end{aligned} \tag{6}$$

where: $\{n\}$ is outward normal vector at the fluid boundary, $\{q\}$ is nodal mass source vector, $\{\dot{q}\}$ is the first time derivative of nodal mass source vector.

At last, the acoustic wave equation in matrix form is presented as:

$$[M_f]\{\ddot{p}\} + [C_f]\{\dot{p}\} + [K_f]\{p\} + \rho_0[R]^T\{\ddot{u}_{e,f}\} = \{F_f\} \tag{7}$$

So, $\left[M_f\right] = \frac{1}{\rho_0 c^2}\iiint\limits_{\Omega_f}\left\{N_p\right\}\left\{N_p\right\}^T dv$ is the acoustic mass matrix; $\left[C_f\right] = \frac{4\mu}{3\rho_0^2 c^2}\iiint\limits_{\Omega_f}\left[\nabla N_p\right]^T\left[\nabla N_p\right]dv$ is the acoustic fluid damping matrix; $\left[K_f\right] = \iiint\limits_{\Omega_f}\frac{1}{\rho_0}\left[\nabla N_p\right]^T\left[\nabla N_p\right]dv$ is the acoustic fluid stiffness matrix; $[R]^T = \oiint\limits_{\Gamma_f}\left\{N_p\right\}\{n\}^T\left\{N'_p\right\}^T ds$ is the acoustic fluid boundary matrix, $\left\{F_{sf}\right\} = -\rho_0[R]^T\left\{\ddot{u}_{e,f}\right\}$. $\left\{F_f\right\} = \iiint\limits_{\Omega_f}\frac{1}{\rho_0}\left\{N_p\right\}\left\{N_p\right\}^T dv\left\{\dot{q}\right\} + \iiint\limits_{\Omega f}\frac{4\mu}{3\rho_0^2 c^2}\left[\nabla N_p\right]^T\left[\nabla N_p\right]dv\{q\}$ is the acoustic fluid load vector

2.2. Fluid-Structure Coupling

The fluid–structure coupled system can be written as:

$$[M_s]\left\{\ddot{u}\right\} + [C_s]\left\{\dot{u}\right\} + [K_s]\{u\} = \{F_s\} + \left\{F_{fs}\right\} \tag{8}$$

$$\left[M_f\right]\left\{\ddot{p}\right\} + \left[C_f\right]\left\{\dot{p}\right\} + \left[K_f\right]\{p\} = \left\{F_f\right\} + \left\{F_{sf}\right\} \tag{9}$$

where $[M_s]$ is the structure mass matrix, $[C_s]$ is the structure damping matrix, $[K_s]$ is the structure stiffness matrix, $\{F_s\}$ is the load vector, $\{F_{fs}\}$ is the force that the fluid exerts on the structure, and $\{u\}$ is the nodal displacement vector. $[M_f]$ is the acoustic mass matrix, $[C_f]$ is the acoustic fluid damping matrix, $[K_f]$ is the acoustic fluid stiffness matrix, $\{F_f\}$ is the acoustic fluid load vector, $\{F_{sf}\}$ is the force that the structure motion produces on the fluid, and $\{p\}$ is the nodal pressure vector.

For natural mode analysis, taking $[C_s] = 0$, $[C_f] = 0$, $\{F_s\} = 0$, and $\{F_f\} = 0$, the following coupled equations are solved:

$$\left[-[M_s]\omega^2 + [K_s]\right]\{u\} = [R]\{p\} \tag{10}$$

$$\left[-\left[M_f\right]\omega^2 + \left[K_f\right]\right]\{p\} = \rho_0[R]^T\omega^2\{u\} \tag{11}$$

where, ω is the frequency, $[R]$ is the acoustic fluid boundary matrix and ρ_0 is the acoustic fluid density constant.

In order to highlight the sound speed c and convenience for the following analysis, the mass matrixes of the fluid part are written out below:

$$\left[M_f\right] = \frac{1}{\rho_0 c^2}\iiint\limits_{\Omega_F}\left\{N_p\right\}\left\{N_p\right\}^T dv = \frac{1}{\rho_0 c^2}\left[\overline{M}_f\right] \tag{12}$$

where $\{N_p\}$ is the element shape function for pressure. Substitute Equation (12) into Equation (11):

$$\left[-\frac{1}{\rho_0 c^2}\left[\overline{M}_f\right]\omega^2 + \left[K_f\right]\right]\{p\} = \rho_0[R]^T\omega^2\{u\}. \tag{13}$$

If p is eliminated from Equations (10) and (11), we have Equation (14), which shows that the speed of sound in the fluid cavity is one of the important factors affecting the added mass:

$$\left[\left([-M_s] - \rho_0[R]\left[-\frac{1}{\rho_0 c^2}\left[\overline{M}_f\right]\omega^2 + K_f\right]^{-1}[R]^T\right)\omega^2 + K_s\right]u = 0. \tag{14}$$

3. Influence of c_c on the First Three Structure Modes

Referring to Liu et al.'s [1] work, a NACA0009 hydrofoil had a truncated chord of 0.1 m and a span of 0.15 m and was made of aluminum with a theoretical density of 2700 kg/m^3, a Young's modulus of 54 GPa, and a Poisson's ratio of 0.3. The cavitation conditions observed during the tests shown in Figure 1a. The 31.8% of the chord is a steady vapor cavity in Liu Xin's work. Therefore, the observed vapor cavity attached to the hydrofoil suction side was modeled with a fluid domain (see Figure 1b) of

constant length (l = 0.0318 m) and constant thickness (h = 0.0018 m) extending throughout the span (b = 0.15 m). For this relatively stable condition, the dynamic change of cavitation was not considered in order to better understand the effect of the sound speed in the cavity on structure dynamics.

The external water had dimensions of 0.15 × 0.15 × 0.3 m. The water density was 1000 kg/m^3. Considering the coupling characteristics of the test system, the inlet and outlet of the fluid were set as the absorbing boundary condition, with an absorption coefficient of 0.3, and the other boundary conditions were set as fully reflective. One side of the hydrofoil was constrained in the fixed surface, and there was a small gap of 1.2 × 10^{-4} m between the opposite side and the tunnel lateral wall.

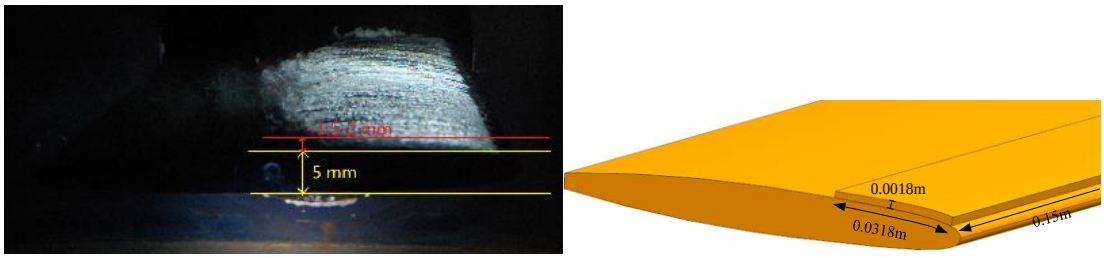

(**a**) (**b**)

Figure 1. (**a**) Photograph of the attached leading edge cavitation during the tests [13]. (**b**) Dimensions and shape of the cavity domain in the numerical model.

When cavitation occurs, the speed of sound in the vapor cavity (c_c) is much lower than that in water. Further, the cavity might not fill with pure water but a mixture of vapor and water. The sound speed inside the cavity may change from less than 10 to 1450 m/s, with the volume fraction of vapor varying within the range of 0–1.0. In this case, simulations were carried out under different sound speeds in the cavity (10–1450 m/s) but with a fixed sound speed (c_f) in the water domain (1450 m/s), and the material properties for the vapor inside the cavity were set to a density of 1.205 kg/m^3.

The variation of the first three modes with sound speed is plotted in Figure 2, where the natural frequencies, f, have been normalized based on Equation (15) to obtain f*:

$$f^* = f \times \mathrm{C}/c_0 \tag{15}$$

where C is the hydrofoil chord length and c_0 is a constant of 1450 m/s

As shown in Figure 2, the submerged structure mode lines in sheet cavitation conditions were named fsc_1–fsc_3. Each color corresponds to the order of the msufferode. The black one (fsc_1) was the first order and had the lowest frequency, followed by the red one (fsc_2) and then the blue one (fsc_3). It can be seen that the structure mode line consisted of two parts: Slash and straight lines. The frequency decreased along the slash lines in a particular range of sonic velocities, and at the same time, the mode shapes also changed. The straight line appeared as a fixed structure mode. The three modes suffered mode transitions. This phenomenon was also found in Liu's paper.

Some typical modes at points B–M are listed in Table 1 to study the mode transition. It can be seen that fsc_3 remained the second bending mode from point A to B on the straight line. When c_c/c_0 = 0.20 at point C, the mode of fsc_3 began to change. At this moment, we defined point C as the mode transition point, which means that the modes began to change. There were many new mode shapes of fsc_3 from point C to J. It can be found that the relative amplitude of the deformation near the mode transition point was high, and that which was away from the mode transition point was low. This also means the mode shapes closer to the mode transition point were easier to excited. Until c_c/c_0 = 0.159 at point I, the vibration amplitude began to increase due to the approach of the next mode transition point K. When c_c/c_0 = 0.131 at point K, fsc_3 changed to the first torsion mode. The second transition line of fsc_3 also had a different slope and mode shape, as shown for point L. With c_c further reducing, the mode fsc_3 became the first bending mode at point M.

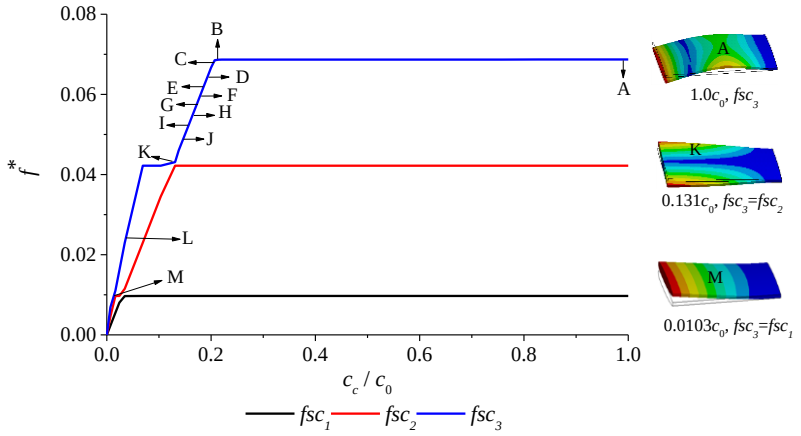

Figure 2. Mode transition lines of the first three structure modes with cavitation.

Table 1. Mode-shapes of points B–M.

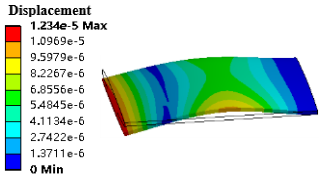	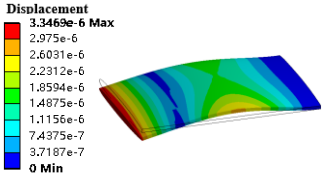	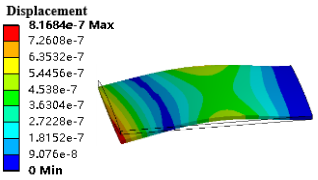
B, $c_c = 0.207c_0, fsc_3 = 1001$ Hz	C, $c_c = 0.2c_0, fsc_3 = 966$ Hz	D, $c_c = 0.192c_0, fsc_3 = 934$ Hz
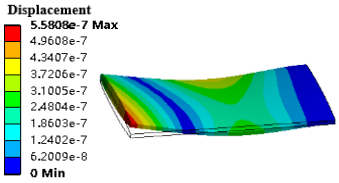	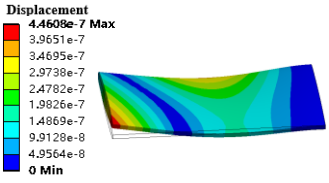	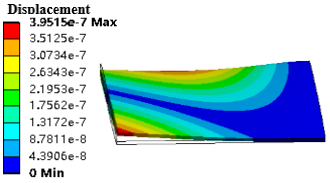
E, $c_c = 0.186c_0, fsc_3 = 901$ Hz	F, $c_c = 0.179c_0, fsc_3 = 867$ Hz	G, $c_c = 0.172c_0, fsc_3 = 834$ Hz
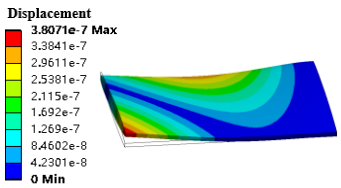	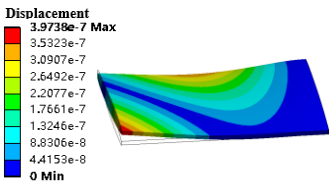	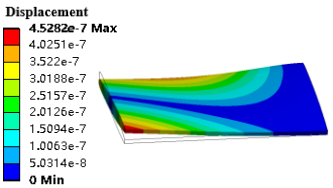
H, $c_c = 0.166c_0, fsc_3 = 800$ Hz	I, $c_c = 0.159c_0, fsc_3 = 734$ Hz	J, $c_c = 0.145c_0, fsc_3 = 701$ Hz
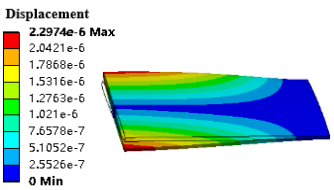	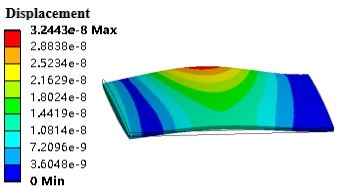	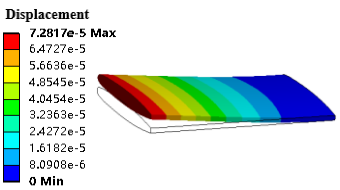
K, $c_c = 0.131c_0, fsc_3 = fsc_2$	L, $c_c = 0.0344c_0, fsc_3 = 333$ Hz	M, $c_c = 0.0103c_0, fsc_3 = fsc_1$

4. Influence of c_c on the Acoustic Modes

The following analysis explains that the abovementioned interesting mode transition phenomenon is related to the acoustic mode of the surrounding fluid. First, the acoustic modes of two cases were calculated and are presented in Figure 3 to show the influence of sonic speed.

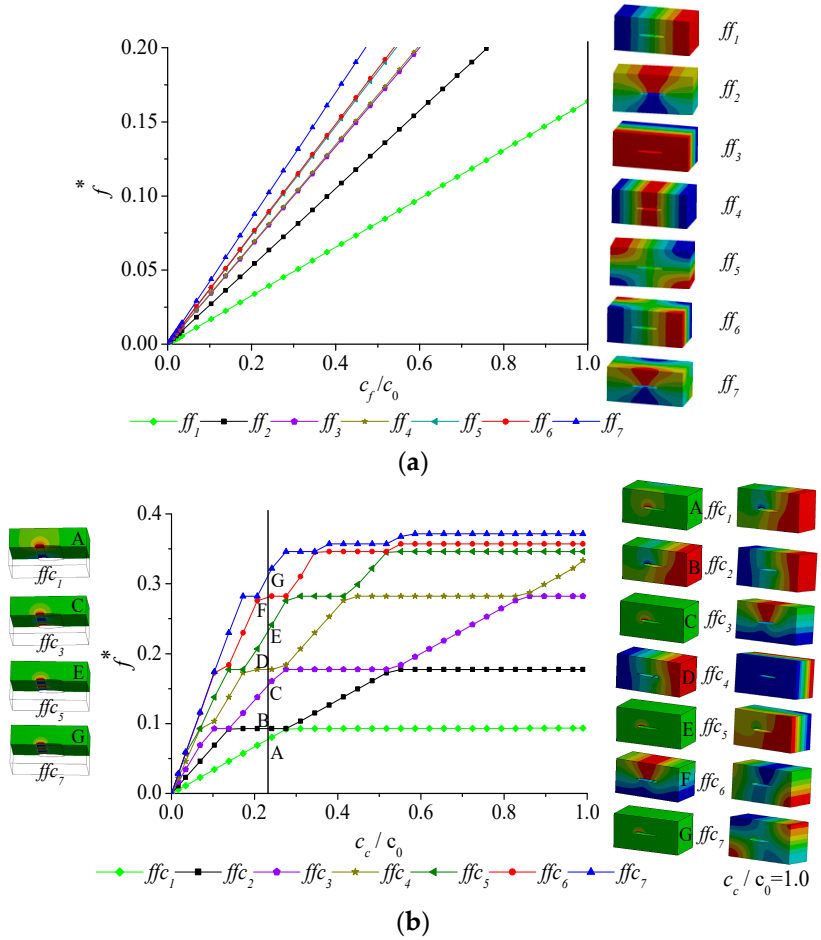

Figure 3. Mode transition lines of the seven first acoustic modes with the (**a**) pure water case and (**b**) cavitation case.

For pure water case (without cavitation), the acoustic modes were calculated with the sound speed in fluid (c_f) domain from 1450 m/s down to 10 m/s. Figure 3a shows that all of the acoustic mode frequencies were in oblique straight lines, and the acoustic modes on each line were the same, as shown on the right side.

However, for the inhomogeneous cavitation case (Figure 3b) with different sound speeds in the cavity (10–1450 m/s) but a fixed sound speed (c_f) in the water domain (1450 m/s), the acoustic mode frequencies were no longer in straight lines but showed many transitions when the sound speed in the cavity changed. Further, many new acoustic modes appeared. For example, if there was a cavity with a density of 1.205 kg/m^3 and a sound speed of 343 m/s according to Brennen 's study, the acoustic modes of points A–G had two types. One included those on the horizontal lines, such as points B (ffc_2), D (ffc_4), and F (ffc_6). For the modes on the horizontal lines, one could find corresponding modes in the pure water case. For example, mode ffc_4 in Figure 3b was similar to ff_1 in Figure 3a, and ffc_6 in Figure 3b was similar to ff_2 in Figure 3a. The other type included those on the slant lines, such as points A (ffc_1), C (ffc_3), E (ffc_5), and G (ffc_7). On these slant lines, new acoustic modes appeared. These modes showed great pressure gradient only near the cavity, as shown on the left side of Figure 3b (to be clear, only the up part is shown). This means that the vapor cavity in water produced new acoustic modes on the slant lines.

In order to find the reason for this difference, simulations with a separated cavity were carried out with $\{u\} = 0$ on the interface between the cavity and water, and the hydrofoil surface was regarded as a rigid boundary. The results are shown in Figure 4. The modes of the separated cavity from fcc_1 to fcc_5 on the leftmost side of Figure 4 changed in lines as the sound speed changed. Further, the acoustical

mode transition lines of water with the cavity coincided with the mode lines of the separated cavity. The first mode transition line was from points A to D in line fcc_1. New mode shapes, such as those at points A–D, were produced by the cavity. The same case was found at points E–I in the second mode transition line fcc_2 and those in other lines. The pressure distribution on the separated cavity was the same as that on the interface between the water and the cavity, which can be clearly observed from the up part of acoustic modes ffc_1–ffc_5. This further confirmed that the existence of a cavity in the fluid domain produced new acoustic modes on the slant lines.

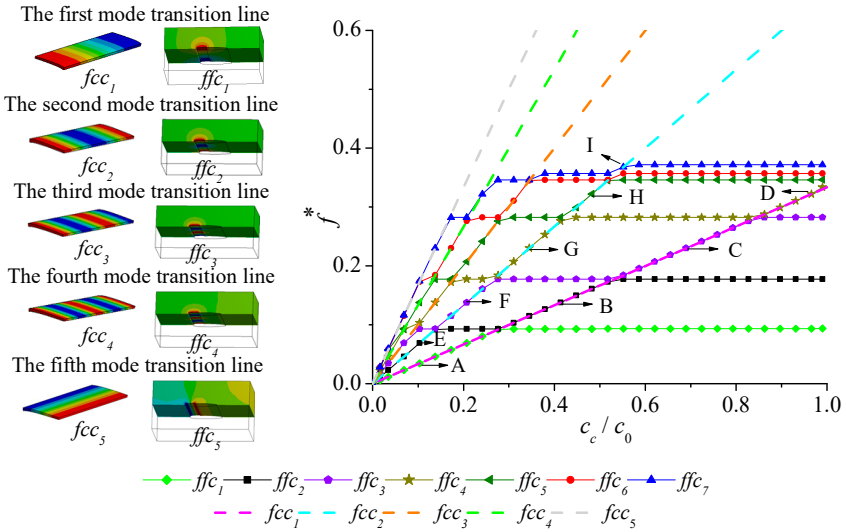

Figure 4. Acoustic modes of separated cavity and water with cavity.

5. Mode Transition and its Relation with Acoustic Modes

The above submerged structure mode lines and the corresponding acoustic modes were put together (Figure 5), where fsc_1–fsc_7 are the first seven order structure modes, and ffc_1–ffc_7 are the first seven order acoustic modes. The acoustic modes with the cavity were not represented by straight lines but did show many transitions. The slant part of acoustic mode line coincided with that of the structure mode line, in which the natural frequencies of the hydrofoil were dominated by the acoustic frequencies and followed their linear decrease. For example, points C–K (Figure 5) were on line ffc_1. Point L in Figure 5 was on line ffc_2. Further, all the mode transition points located where the acoustic frequency was close to the structure mode under the c_c/c_0 = 1.0 condition. Since the acoustic mode transitions, many structure transitions were observed. The conclusion can be drawn that the acoustic mode transition was the reason for the mode transition of the structure surrounded by water with the cavity.

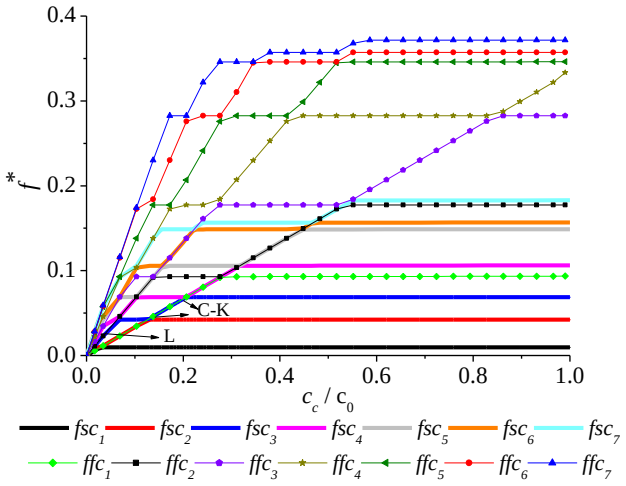

Figure 5. Mode transition lines of not fully wetted structure with varying sound speeds (c_c) in the cavity.

The structure mode shape in the transition line was more complicated and varied with the sound speed. For example, points C–K were on the same transition line, but they showed obviously different mode shapes (Table 1). This was because the acoustic mode also exhibited mode transition caused by the cavity in water. Many new acoustic modes appeared and the mode shapes changed with the sound speed.

A detailed comparison of the structure and acoustic modes is shown in Table 2 for points E, I, and L. It can be seen that the movements of the structure were mainly affected by the pressure distribution of the newly added acoustic mode. The acoustic mode on the interface between the cavity and the hydrofoil surface of points E and I showed high pressure fluctuations with the reversed phase on two corners near the hydrofoil leading edge, which induced the structure mode of the second bending mode. Also, the inhomogeneous pressure distribution at the inlet and outlet sides of the hydrofoil caused torsional movement. So, bending–torsion coupled modes appeared in points E and I. As shown in Table 2, the acoustic modes on points E and I appeared to be almost the same. However, when they coupled with structure modes, obviously different pressure distributions appeared between points E and I, as shown by second row in Table 2. Therefore, the slight difference between the acoustic mode on points E and I made the structure mode on point I behave more torsionally than on point E, while on point L, the pressure fluctuation in the middle of the leading edge had the opposite phase as that at the two ends. Thus, the structure mode on point L looked like the second bending movement. It can be concluded that the acoustic pressure mode that changed with the varying c_c caused a different structure mode on the transition line.

Table 2. Structure and acoustic modes on the hydrofoil surface on points E, I, and L.

Modes	E, 0.186c_0	I, 0.159c_0	L, 0.034c_0
Structure mode (FSI, Fluid-structure interaction)	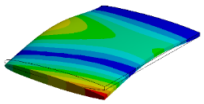	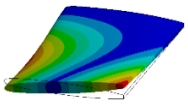	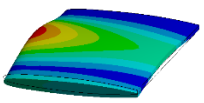
Acoustic mode (FSI)	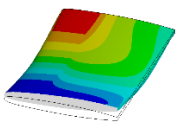	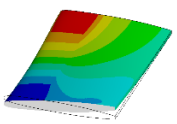	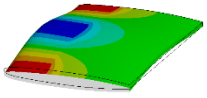
Acoustic mode (without coupling)	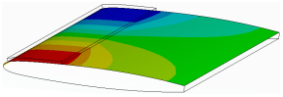	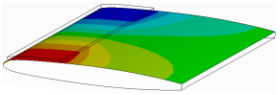	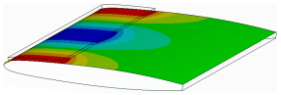

6. Verification of the Case in Real Cavitation Conditions

De La Torre et al. [15] experimentally observed that the mode shape of the second bending mode under cavitation conditions was actually closer to a bending–torsion coupled mode, but the reason for this was not explained. Based on the abovementioned study, we further discuss the experimental case. Figure 6 shows the hydrofoil used in experiments. A stable cavity of 50% of the chord could be obtained when the flow velocity was fixed at 11.8 m/s in De La Torre et al.'s (2015) experiment. Meanwhile, the relative amplitudes of 26 points on the hydrofoil were measured, as shown in Figure 7. The distance between points was 0.02 and 0.025 m in the chord-wise and span-wise directions, respectively, except that points 1, 7, 11, 17, and 21 were 0.018 m.

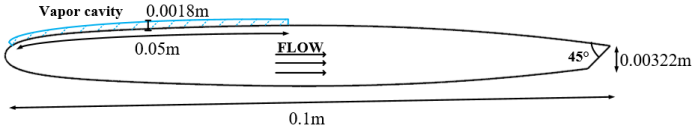

Figure 6. Cross section of the hydrofoil from the leading edge (left) to the trailing edge (right).

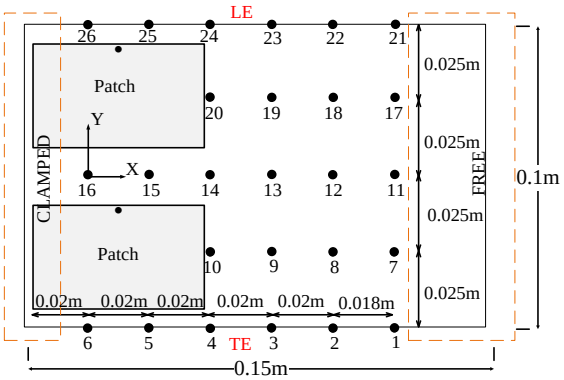

Figure 7. Top view of the hydrofoil and measurement points on the surface [15].

In real cavitation conditions, the inside of the cavity was a mixture of vapor and water. As taken from Brennen [3], the sound speed in a mixture of water and vapor varies with the void fraction α. The attached cavity morphology was not homogeneous. We defined the vapor cavity as pure vapor (α = 1.0) with a density of 1.205 kg/m^3 and a sound speed of 343 m/s, and the predicted mode shapes are shown on the right side of Figure 8 in comparison with the experimental mode. The measured points only covered part of the foil, which correspond to the red dashed area in the row labeled "Sim.". The yellow dashed line represents the node line of the mode shape where the displacement was zero. It was clearly observed that the predicted node line of the first bending mode (A_1, fsc_1) and the torsion mode (B_1, fsc_2) was consistent with the experimental results. For the second bending mode (C_1, fsc_3), the two predicted node lines were both parallel to the clamped section, which showed a pure second bending mode, not the expected bending–torsion coupled mode obtained from experiments, and the frequency of 1017 Hz was larger than the experimental value shown in Table 3. In this calculation case, the acoustic mode of the cavity had no influence on the three structure modes because the first acoustic mode frequency is higher than that of the third structure line shown in Figure 5.

However, when the α decreased to 0.999 with a density of 2.3 kg/m^3 and a sound speed of 275 m/s, the mode at points A_2 and B_2 remained as the first bending mode (fsc_1) and the first torsional mode (fsc_2). However, for point C_2, the two predicted node lines were consistent with the experimental results, showing a bending–torsion coupled mode shape because the third mode at C_2 was near the mode transition point. Further, the predicted frequency was 960 Hz at point C_2, with a deviation of only -0.1% compared with the experimental value of 961 Hz.

Table 3. Numerical and experimental natural frequencies under cavitation conditions.

Modes	First Bending fsc_1	Torsion fsc_2	Second Bending fsc_3
Exp. (Hz)	134	670	961
Sim. (Hz)	139	647	1017
Dev. (%)	3.7	-3.5	5.8

More precisely, a line close to the trailing edge was selected to quantify the mode shape changes (Figure 9). With the decrease of α, the zero displacement location moved backwards towards the hydrofoil clamped section. When the α reduced from 1.0 to 0.999, the deviations of the predicted node to experimental node reduced from 6.42% to 2.75%. The relative amplitudes of the first bending mode (fsc_1), the torsion mode (fsc_2), and the second bending mode (fsc_3) under α = 0.999 are shown in Figure 10 and compared with the measured ones. They showed good agreement except for slight deviations on some points.

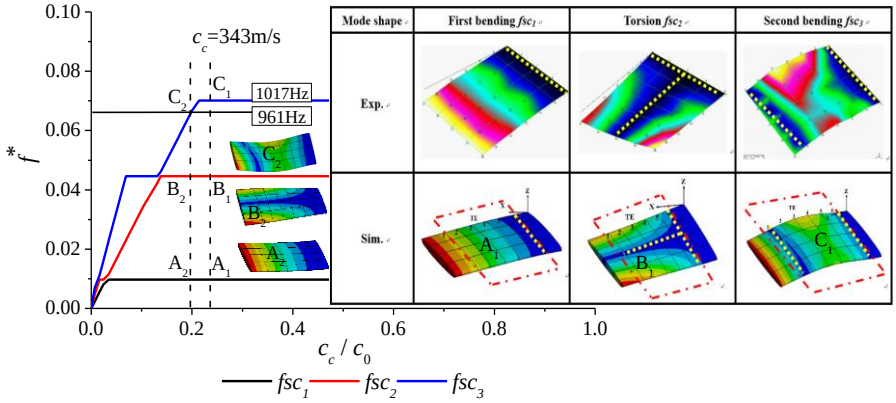

Figure 8. Mode shape changes with different void ratio α.

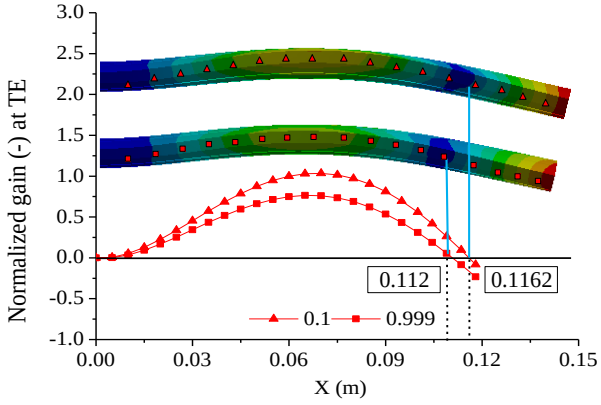

(**a**)

α	α=1.0	α=0.999
Experiment (m)	0.109	0.109
Simulation (m)	0.116	0.112
Deviation (%)	6.42	2.75

(**b**)

Figure 9. The displacement line on the trailing edge of second bending mode fsc_3 with different cavity void ratios α. (**a**) The changes of displacement line. (**b**) Experimental and numerical displacement line and percent deviations with varying α in cavity.

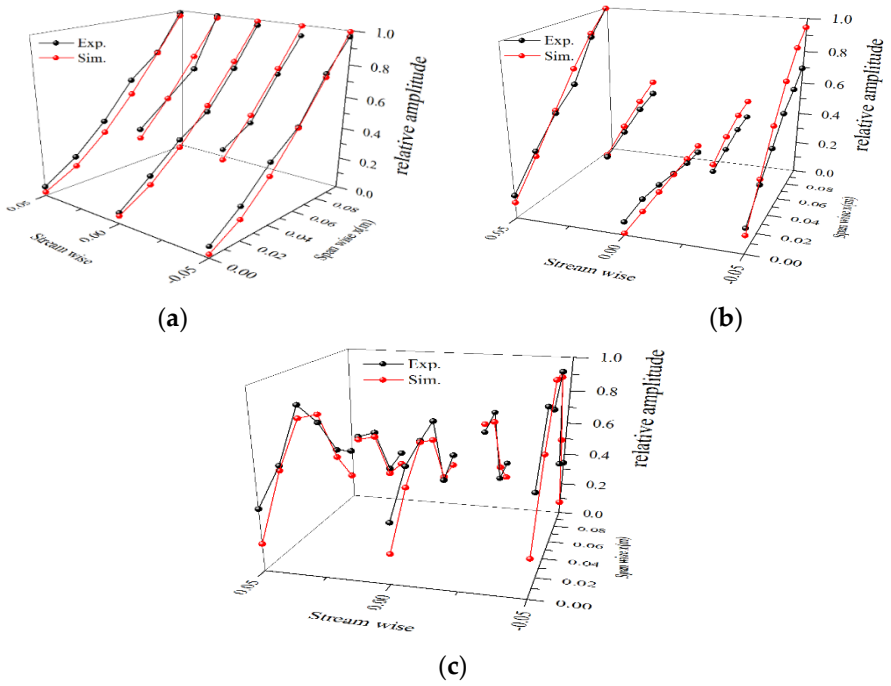

Figure 10. Comparison of numerical and experimental mode shapes for fs_1, fsc_2 and fsc_3 in cavitation. (**a**) First bending fsc_1 in cavitation. (**b**) First torsion fsc_2 in cavitation. (**c**) Second bending fsc_3 in cavitation. Experimental and numerical displacement and percent deviations for cavitation conditions.

7. Conclusions

The influence of sound speed in the vapor cavity (c_c) on the structure mode was investigated numerically in this paper. An attached sheet cavity was simulated with a varying sonic speed c_c (10–1450 m/s) in the cavity but a fixed sound speed c_f in water (1450 m/s). Based on the results, the following conclusions can be drawn:

1. The structure mode undergoes mode transition phenomenon when the acoustic frequency is close to the structure mode under a c_c/c_0 = 1.0 condition. It can be seen that the amplitude of the vibration near the mode transition point is high. In this case, the mode shape is more easily motivated.
2. The acoustic mode also suffers from mode transitions and produces some new acoustic modes because of the variation of sound speed in the cavity. The mode transition phenomenon of the structure is caused by the coupling of the structure mode with the acoustic mode. Therefore, the structure mode shape in the transition line is more complicated and varies with the sound speed since the cavity inside the water induces new acoustic modes and the mode shapes change with the sound speed.
3. The sheet cavity is composed of a mixture of liquid and vapor phases and even a very small fraction of vapor may cause a great change in the speed of sound inside the cavity, this induces a new acoustic mode, and the coupling of the structure and acoustic modes may change some lower-order mode shapes. If the void fraction α changes from 1.0 to 0.999, the sound speed will change from 343 to 275 m/s, which will cause a new mode shape to appear between the second bending and the first torsional mode, which is in agreement with the experimental results. So, for the structural dynamic analysis of real hydraulic machinery, great care must be taken when cavitation occurs.

Author Contributions: Methodology, L.Z.; investigation, W.W.; writing-original draft preparation, W.W.; writing—review & editing, L.Z. and X. E; supervision, O.T.; funding acquisition, L.Z.

Funding: This research was funded by the National Natural Science Foundation of China (No. 51479200).

Conflicts of Interest: The authors declare no conflict of interest.

References

1. Liu, X.; Zhou, L.J.; Escaler, X.; Wang, Z.W.; Luo, Y.Y.; De La Torre, O. Numerical simulation of added mass effects on a hydrofoil in cavitating flow using acoustic FSI. *J. Fluids Eng.* **2017**, *139*, 041301. [CrossRef]
2. Blevins, R.D.; Plunkett, R. Formulas for Natural Frequency and Mode Shape. *J. Appl. Mech.* **1979**, *47*, 461. [CrossRef]
3. Brennen, C.E. *Homogeneous Bubbly Flows, Cavitation and Bubble Dynamics*; Oxford University Press: Oxford, UK, 1995.
4. Fu, Y.; Price, W.G. Interactions between a partially or totally immersed vibrating cantilever plate and the surrounding fluid. *J. Sound Vib.* **1987**, *118*, 495–513. [CrossRef]
5. Lindholm, U.; Kana, D.; Chu, W.; Abramson, H.; Norman, H. Elastic vibration characteristics of cantilever plates in water. *J. Ship Res.* **1965**, *9*, 11–29.
6. Kwak, M.K. Vibration of circular plates in contact with water. *J. Appl. Mech.* **1991**, *58*, 480–483. [CrossRef]
7. Chang, T.; Liu, M. On the natural frequency of a rectangular isotropic plate in contact with fluid. *J. Sound Vib.* **2000**, *236*, 547–553. [CrossRef]
8. Ergin, A.; Ugurlu, B. Linear vibration analysis of cantilever plates partially submerged in fluid. *J. Fluids Struct.* **2003**, *17*, 927–939. [CrossRef]
9. Dompierre, F.; Sabourin, M.; Pelletier, D. Simulation of structure vibration in water. In Proceedings of the IOP Conference Series: Earth and Environmental Science, Do Iguassu, Brazil, 27–31 October 2008.
10. Rodriguez, C.; Egusquiza, E.; Escaler, X.; Liang, Q.; Avellan, F. Experimental investigation of added mass effects on a Francis turbine runner in still water. *J. Fluids Struct.* **2006**, *22*, 699–712. [CrossRef]
11. Valentín, D.; Presas, A.; Egusquiza, E.; Valero, C. Experimental study on the added mass and damping of a disk submerged in a partially fluid-filled tank with small radial confinement. *J. Fluids Struct.* **2014**, *50*, 1–17. [CrossRef]
12. Fine, N.E.; Uhlman, J.S.; Kring, D.C. Calculation of the added mass and damping forces on supercavitating bodies. In Proceedings of the Fourth International Symposium on Cavitation (CAV 2001), Pasadena, CA, USA, 20–23 June 2001.
13. Torre, O.D.L.; Escaler, X.; Egusquiza, E.; Farhat, M. Experimental investigation of added mass effects on a hydrofoil under cavitation conditions. *J. Fluids Struct.* **2013**, *39*, 173–187. [CrossRef]
14. Torre, O.D.L.; Escaler, X.; Egusquiza, E.; Farhat, M. Numerical and experimental study of a nearby solid boundary and partial submergence effects on hydrofoil added mass. *Comput. Fluids* **2014**, *91*, 1–9. [CrossRef]
15. Torre, O.D.L.; Escaler, X.; Egusquiza, E.; Farhat, M. Experimental mode shape determination of a cantilevered hydrofoil under different flow conditions. *Proc. Inst. Mech. Eng. Part C J. Mech. Eng. Sci.* **2016**, *230*, 3408–3419. [CrossRef]
16. Liu, X.; Wang, Z.W.; Escaler, X.; Zhou, L.J. Numerical evaluation of cavitation void ratio significance on hydrofoil dynamic response. *J. Phys. Conf. Ser.* **2015**, *656*, 012159. [CrossRef]
17. Bossio, M.; Valentín, D.; Presas, A.; Martin, D.R.; Egusquiza, E.; Valero, C.; Egusquiza, E. Numerical study on the influence of acoustic natural frequencies on the dynamic behaviour of submerged and confined disk-like structures. *J. Fluids Struct.* **2017**, *73*, 53–69. [CrossRef]